Deterministic stochastic resonance in a Rössler oscillator

Kenichi Arai, Shin Mizutani, and Kazuyuki Yoshimura
NTT Communication Science Laboratories, 2-4, Hikaridai, Seika-cho, Soraku-gun, Kyoto 619-0237, Japan
(Received 15 August 2003; published 24 February 2004)

We discuss the characteristics of stochastic resonancelike behavior observed in a deterministic system. If a periodically forced Rössler oscillator strays from the phase locking state, it exhibits the intermittent behavior known as phase slips. When the periodic force is modulated by a weak signal, the phase slips synchronize with the weak signal statistically. We numerically demonstrate, in terms of interslip intervals and signal to noise ratio, that the maximum synchronization can be achieved with the optimum intensity of chaotic fluctuations. It is shown that the stochastic resonancelike behavior can be observed regardless of the choice of parameters. The frequency dependence of the signal indicates that there is an optimum frequency for the maximum resonance. The phase slip rate is derived based on the fact that the phase slips are caused by a boundary crisis caused by an unstable-unstable pair bifurcation. The interslip distributions obtained from the derived slip rate and the approximation theory of the time-dependent Poisson process agree with those obtained by numerical simulations. In addition, the maximum enhancement of a weak signal is shown to be achieved by adjusting the chaotic fluctuations even if a signal becomes mixed with noise.

DOI: 10.1103/PhysRevE.69.026203 PACS number(s): 05.45.Xt, 05.45.Pq, 02.50.Ey

I. INTRODUCTION

Stochastic resonance (SR) has been a subject of great interest in nonlinear physics since the concept of SR was first proposed in answer to questions about the periodically recurrent ice ages [1–3]. SR has been considered a counterintuitive phenomenon: the maximum enhancement of a weak periodic signal buried in noise can be achieved with a nonzero optimum amount of noise although it is usually thought to be easier to detect a weak signal when the noise is smaller. The mechanisms of the SR effects have been elucidated by many theoretical approaches (see Refs. [4–7] and references therein). On the other hand, SR has been studied experimentally in various kinds of systems including electrical, optical, and neuronal systems (see Ref. [4] and references therein). In particular, SR has come to be significant for sensory neuronal systems since it is believed to be used by sensory neurons to detect a weak signal in a real noisy environment [8].

Most SR studies have been carried out on bistable or multistable systems, typically realized by an overdamped particle driven by periodic and random forces in a double-well potential. Some dynamical systems possessing a single stable point and a reinjection dynamical process, where after escaping from the stable point, a trajectory returns to the stable point deterministically, have the potential to yield SR and they form another important class of SR. The typical realization of this kind of dynamics is given by the equation $d\theta/dt = A + \sin\theta$ and FitzHugh-Nagumo (FHN) models [9,10], which can describe the dynamics in Josephson devices or sensory neurons, respectively. In fact, some SR studies have been based on the FHN model in order to understand the mechanisms of biological sensory systems because it is believed that sensory neurons utilize the SR effect in a noisy environment [11,12].

Meanwhile a number of studies on SR have been carried out for systems with deterministic noise, that is, chaotic fluctuation. It is natural to look for SR-like phenomena in a deterministic chaotic system since chaotic fluctuation is similar to noise on a coarse-grained time scale. In fact, a number of SR-like phenomena in chaotic systems have been reported. One approach consists of adding the chaotic forcing generated by a logistic map to a double-well system along with a harmonic signal and observing the SR fingerprint [13]: the dependence of SNR versus the amplitude of the chaotic forcing has a bell-shaped maximum. Another sort of SR-like phenomenon has been reported in terms of the intermittent hopping between two chaotic states such as two wells of a periodically forced double-well Duffing oscillator [14], two phases of a period-doubled single-well Duffing oscillator [15,16], two single scrolls of Chua's circuit with a harmonic signal [17,18], two chaotic repellers in a periodically modulated cubic map [19], two formerly disjoint attractors in a one-dimensional piecewise-linear map [20], and two symmetric attractors in a Lorenz model [19]. These reports showed that the intermittent events resonate with the signal and the resonance can be maximized by the chaotic fluctuation. Some authors discussed more effective methods for signal enhancement by SR-like phenomena in chaotic systems [18,21,22]. In addition, SR-like phenomena have been experimentally observed in noiseless systems such as chaotic spin-wave dynamics [23] and a CO_2 laser [24].

Few SR-like phenomena have been found for monostable chaotic systems with a reinjection mechanism. We demonstrated SR-like behavior in chaotic systems with a reinjection mechanism, employing a forced Rössler oscillator, and the SR-like behavior in a deterministic chaotic system is referred to as *deterministic* stochastic resonance (DSR) [25]. In this paper, we focus on phase slips, which are intermittent 2π phase jumps in quasiphase synchronization, and report the correspondence between *interslip interval distribution* (ISID) and the residence-time distribution in SR. In addition, we show that the *signal to noise ratio* (SNR) behavior coincides with that of SR. We also describe some properties of these phenomena.

Certain authors have pointed out a relationship between a crisis and DSR [15,16,19,26]. Lately, we have described the

dynamical mechanism of DSR, that is, a theoretical explanation of DSR in terms of its dynamics [25]. In this paper, we refine the previous explanation in that we show the part played by a boundary crisis in the occurrence of DSR and that the bifurcation parameters of the crisis play central roles as regards inputing a signal and controlling fluctuation in DSR. We specifically emphasize that the DSR mechanism can be explained using the scaling law of bifurcation parameters and a Poisson process approximation.

We show that DSR-like behavior can be observed even if a signal is mixed with noise: the maximum enhancement of a weak signal can be achieved by adjusting the internal fluctuation depending on the noise intensity. This phenomenon is called noisy DSR.

This paper is organized as follows. In Sec. II, we introduce some of the basic characteristics of phase synchronization and phase slips, which appear just after the phase synchronization is broken. We numerically demonstrate DSR and show some of its characteristics in Sec. III. Then, we explain the dynamical origin of DSR in Sec. IV, applying the scaling law of the crisis and the Poisson process approximation. In Sec. V, we report the DSR-like behavior that occurs when a signal is contaminated with noise. Finally, we provide the conclusion in Sec. VI.

II. PHASE SLIP

A. Phase synchronization of Rössler oscillator

Let us consider a Rössler oscillator driven by a sinusoidal force:

$$\dot{x} = -\nu y - z,$$

$$\dot{y} = \nu x + a y + K \sin(\Omega t), \tag{1}$$

$$\dot{z} = b + z(x - c),$$

where $a=0.2$, $b=0.2$, and $c=4.8$ and K, Ω, and ν can be varied depending on the situation. With a small K, this dynamical system yields a chaotic attractor similar to the original nonforcing one and its trajectories rotate around the z axis.

Frequency locking in a chaotic system can be described in terms of the observed mean angle velocity

$$\bar{\Omega} = \lim_{t\to\infty} 2\pi \frac{N_t}{t}, \tag{2}$$

where N_t is the number of intersections between a trajectory and a reference surface such as a half-plane ($y=0$ and $x>0$), during an observation interval t. Figure 1 shows the angle velocity difference $\Delta\Omega = \bar{\Omega} - \Omega$ between the Rössler oscillator and the external force as a function of Ω and K. We can see the plateau region where the difference $\Delta\Omega$ is zero, where the oscillator frequency is locked by the external force. It is noted that this figure is similar to the one obtained for the synchronization of periodic oscillators.

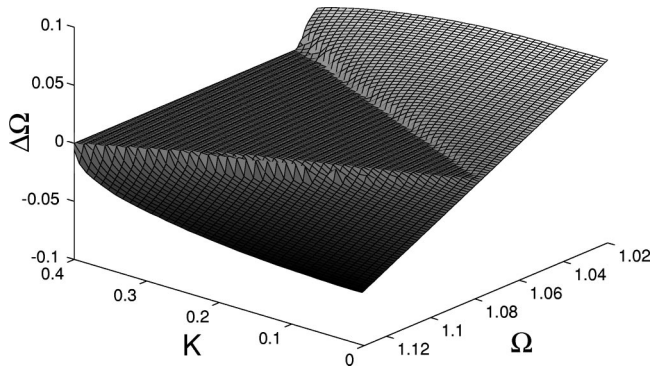

FIG. 1. Mean angular velocity difference $\Delta\Omega$ between the Rössler oscillator and the forcing frequencies is plotted as a function of the coupling strength K and the forcing period Ω with $\nu = 1.0$. In the plateau region, the frequency of the Rössler oscillator is locked to that of the external force.

The phase of an oscillator has to be defined in order to describe a phase synchronization [27]. However, in general it is difficult to define the phases of chaotic rotations. Nevertheless, since we employ only proper Rössler oscillators, namely, their trajectories rotate around the z axis, we can use the angle variable,

$$\theta = \arctan\frac{y}{x}, \tag{3}$$

as the phase, satisfying the following conditions for the phase: the phase is set at $2\pi n$ ($n=0,1,2,\ldots$) on the reference plane and the phase of a rotation monotonically increases with time. Let the θ value be continuous with respect to time: i.e., integer multiples of 2π differences in θ are distinguished. It should be noted that the mean angle velocity obtained by the angle variable is asymptotically coincident with that obtained by Eq. (2). Since a cylindrical coordinate is useful for the following discussion, we introduce the amplitude of rotations: $r=\sqrt{x^2+y^2}$.

When the Rössler oscillator is not synchronized with the forcing, the largest Lyapunov exponent has a positive value and the second exponent is practically zero. Roughly speaking, the second exponent corresponds to the angle variable. Due to chaotic fluctuation, the angle variable diffuses as a fractional Brownian motion with the drift $\bar{\Omega}t$ [28]. The Hurst exponent of our chaotic diffusion is almost exactly 0.5 as shown in Fig. 2 and so the diffusion can be regarded as an ordinary Brownian motion.

When the forcing strength K becomes large or the external frequency Ω approaches $\bar{\Omega}$, the second exponent becomes negative and then the phase diffusion is suppressed. Hereafter, let us focus on the phase difference $\Delta\theta$ between the Rössler oscillator and the external force

$$\Delta\theta = \theta - \Omega t. \tag{4}$$

In Fig. 3, we can see that $\Delta\theta$ with $K=0.15$ is almost constant while the force is insufficiently strong to restrain the chaotic fluctuation of the amplitudes, where $\Omega=1.0077$ and

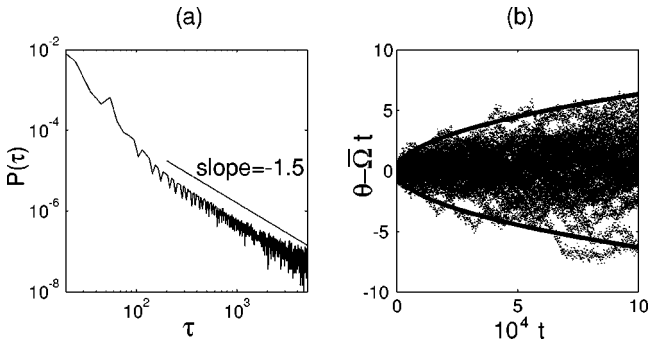

FIG. 2. (a) Probability distribution of the first-return time of $\theta - \bar{\Omega} t$. The slope of the distribution for large τ is -1.5 and so the Hurst exponent is almost exactly 0.5. (b) The phase difference $\theta - \bar{\Omega} t$ of the 50 example trajectories is plotted when $\nu = 1.0$, $\Omega = 1.077$, $K = 0.001$, and $\bar{\Omega} = 1.077\,46$. The solid line shows $\pm 0.020 \times \sqrt{t}$, and we can see that the diffusion of the difference is proportional to $\sqrt{t}$. These figures confirm that the phases diffuse in a way that is similar to a Brownian motion.

$\nu = 1.0038$. This is called chaotic phase synchronization. Chaotic phase synchronization can be observed if K is larger than a critical value K_c, which is 0.1403 when $\Omega = 1.0077$ and $\nu = 1.0038$. Hereafter, $\Omega = 1.0077$ and $\nu = 1.0038$ unless otherwise mentioned.

B. Demonstration of phase slip

When K is smaller than the critical value K_c, $\Delta\theta$ increases with intermittent 2π jumps although $\Delta\theta$ is almost constant except for these jumps, as shown in Fig. 3 for $K = 0.035$ and 0.036. This is called a phase slip [29–32]. It should be noted that the K values employed in the experiments are much smaller than the critical value since much longer intervals are needed to observe phase slips with K close to the critical value. In addition, we modified the Rössler oscillator in order to see a sufficiently large number of phase slips as follows:

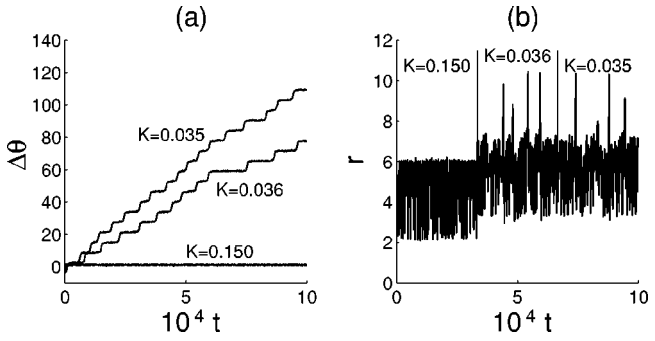

FIG. 3. Plot of phase differences between the Rössler oscillator and the external force (a) and amplitudes (b) when $\nu = 1.0038$, $\Omega = 1.0077$, and $\alpha = 0.0$. With $K = 0.15$, the phase difference is almost constant, which indicates the phase synchronization, while the behavior of the amplitude remains chaotic. With $K = 0.0035$ and 0.0036, phase slips (intermittent phase jumps) are observed. We can see the more phase slips with $K = 0.0035$ than with $K = 0.0036$.

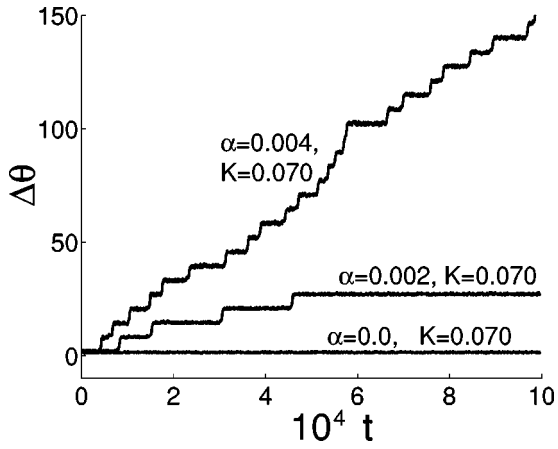

FIG. 4. Phase slips for $\alpha = 0.0$, 0.0020, and 0.0040 with $\nu = 1.0038$ and $\Omega = 1.0077$. More phase slips occur as α increases.

$$\dot{x} = s(-\nu y - z),$$

$$\dot{y} = s(\nu x + a y) + K \sin(\Omega t), \tag{5}$$

$$\dot{z} = s[b + z(x - c)],$$

where $s = 1 + \alpha(r^2 - \bar{r^2})$ and $\bar{r}$ is the average r value for an ordinary Rössler oscillator, i.e., $\alpha = K = 0$. The positive scalar factor s on the right-hand side of Eq. (5) affects the motion of a state point so that the state point is accelerated far from the origin and decelerated near the origin. Thus, the factor s enlarges the fluctuation of the angular velocity, driven by the fluctuation of the amplitude. Therefore, as α increases, the fluctuation of the angular velocity increases. Figure 4 shows the time courses of $\Delta\theta$ for certain values of α and confirms that phase slips occur more frequently as α increases. In the following, $\alpha = 0.002$.

III. DEMONSTRATION OF DETERMINISTIC STOCHASTIC RESONANCE

In this section, we demonstrate DSR, using a modified Rössler oscillator driven by a periodical force whose coupling is modulated by a weak signal

$$\dot{x} = s(-\nu y - z),$$

$$\dot{y} = s(\nu x + a y) + K[1 + \epsilon \sin(\omega t)]\sin(\Omega t), \tag{6}$$

$$\dot{z} = s[b + z(x - c)],$$

where, with a modulation signal, $\epsilon = 0.05$ and $\omega = 6.0 \times 10^{-4}$ unless otherwise mentioned. It should be noted that the modulation signal is much slower than the chaotic oscillation and the external forcing. While noise, together with a periodic signal, is added to a system to observe ordinary SR, only a periodic signal is inputed into a system to observe DSR since the chaotic fluctuation itself acts like noise. Here, the signal is inputed using a method whereby the amplitude of external forcing is modulated. The frequency modulation can also be employed and both are compared in Ref. [18].

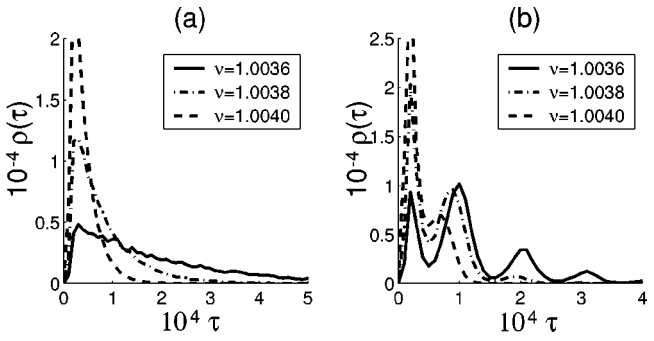

FIG. 5. Probability distribution of interslip intervals with $K=0.070$. (a) Without a signal, the distributions form exponential tails except when τ is small. As ν increases, the distribution becomes steep, in other words, the mean interslip interval becomes small. (b) When the coupling strength is modulated by a signal, there are multipeaks centered at integer multiples of the period $2\pi/\omega$ ($\simeq 1.047\times 10^4$) of the modulation signal.

Several measures of SR have been developed over the past decade. It has become common to quantify SR by using SNR, which describes the quality of a signal in the presence of background noise. An analytical expression of SNR is found in Ref. [11]. While an SNR curve has a resonance-like shape as a function of noise level, it does not have a maximum when the frequency of driving force is varied. Other measures of SR, based on the residence-time distribution of a bistable, periodically driven system, have been introduced to characterize SR [33,34]. Longtin *et al.* compared the interspike interval histograms of sinusoidally stimulated auditory nerve from cat with return-time distribution of the periodically driven bistable system [35]. Zhou *et al.* studied the heights of peaks in the residence-time distribution at odd multiples of the half-period of the driving force [36]. The peak heights pass through a maximum as a function of noise intensity. Gammaitoni *et al.* [37] introduced the area under the peak of the residence-time distribution at the half-period of the driving force as a measure for SR. In addition, they have shown that the area passes through a maximum as a function of the driving frequency as well as the noise level. It should be noted that the noise strength that maximizes the area under the peak does not match the noise level that maximizes the SNR. The analytical expressions of the residence-time distribution have been provided by Choi *et al.* [38]. Other sorts of quantities for characterizing SR have been discussed. A correlation function was introduced for SR-type behavior with aperiodic input signals [39]. Goychuk [40] found an analytic expression for the rate of information gain and showed that it is proportional to SNR when the signal is weak. Since we focus on intermittent events, namely, phase slips, in time series, we mainly employ the interslip interval distribution ISID to quantify DSR. In addition, we may safely say that ISID has advantages as regards discussing SR-type behavior when the frequency of external force is varied.

A. Interslip interval distribution (ISID)

Figure 5 shows the probability distribution $\rho(\tau)$ of interslip intervals, which are the durations between two consecutive slips for $\epsilon=0$ (a) and $\epsilon=0.05$ (b). Without a modulation signal (i.e., $\epsilon=0$), the ISID is unimodal and decays exponentially for a large τ. The figure shows that the ISID deviates from the exponential form in the small τ range: phase slips cannot occur in a short-period succession and it is considered that there is some refractory time. The exponential form, i.e., $\rho(\tau)\simeq\lambda\exp(-\lambda\tau)$, in the large τ range implies that the occurrence of phase slips is well approximated by a Poisson process: successive phase slips are statistically independent and the probability of a phase slip occurring during a short period Δt is given by $\lambda\Delta t$, with no memory. λ indicates the index of the exponential distribution, which can be estimated by the mean phase slip rate, and this grows as K decreases or ν increases in the parameter range we used.

A small modulation signal causes a slight change in the shape of the attractor, compared with a nonsignal attractor. However, the ISID $\rho_\epsilon(\tau)$ changes greatly, in other words, it develops multipeaks as shown in Fig. 5(b) for several ν values. The peaks are centered at integer multiples of the period $2\pi/\omega$ of the modulation signal. In addition, we can see that the heights of these peaks decrease exponentially with their order. These results are very similar to the residence-time distribution of SR in excitable systems and imply that phase slips occur in statistical synchronization with the modulation signal. The phase slips are most likely to occur for a certain phase of the modulation signal: the maximum probability for a phase slip visits every period of the modulation signal. If the system misses the first good chance to slip, it has another good opportunity after one cycle and so on.

Although the system has no stochastic features, it behaves as if it were a stochastic system due to the chaotic fluctuation. We have to vary the intensity of the chaotic fluctuation rather than that of the noise in order to confirm the existence of SR-like phenomena in the Rössler oscillator, namely, the bell-shaped peak height of the ISID as a function of the chaotic fluctuation. We saw that the parameter values, ν or K, change the phase slip rates and we consider that the phase slip rates are determined by the intensity of the internal fluctuation. This implies that by adjusting the ν or K value, we can control the system fluctuation. It should be noted that although ν was often employed for controlling the phase slip rates rather than K in these experiments, ν can play the same role as K.

Figure 6 shows $\Delta\rho_n$ obtained numerically as a function of ν to verify the SR-like behavior. $\Delta\rho_n$ indicates the difference between the nth peak heights in the ISID with and without a modulation signal: $\Delta\rho_n(\nu)=\rho(\tau_n;\nu,\epsilon=0.05)-\rho(\tau_n;\nu,\epsilon=0)$ where, for a given ν value, $\rho(\tau_n;\nu,\epsilon=0.05)$ and $\rho(\tau_n;\nu,\epsilon=0)$ represent the peak height in the ISID for $\epsilon=0.05$ and $\epsilon=0$, respectively, at $\tau_n=2\pi n/\omega$. Here, we consider that the phase slips without a modulation signal are caused by background noise and then the nonsignal ISID should be subtracted from the ISID with the modulation signal. The difference $\Delta\rho_1$ for the first peak increases until it reaches a maximum value at $\nu\simeq 1.0038$ and then decreases monotonically. For the second peak, $\Delta\rho_2$ also has a unimodal shape and it has a maximum point at $\nu\simeq 1.0036$, which is smaller than ν for $\Delta\rho_1$. Since the peak heights $\Delta\rho_1$ can be

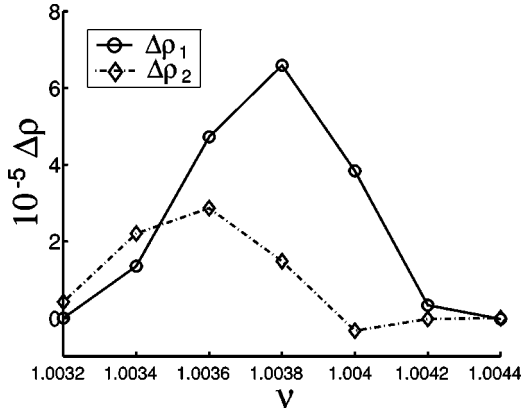

FIG. 6. The peak height difference $\Delta\rho_n(\nu)$ is plotted vs ν for $n=1,2$ with $K=0.070$. Each curve has a bell-shaped maximum and this coincides with the SR characteristics.

regarded as the magnitude of the resonance, Fig. 6 means that the system resonates most with the modulation signal at the optimum ν values. In other words, the optimum coherent behavior with the signal is achieved for an appropriate intensity of internal randomness. It should be emphasized that this resonant behavior in $\Delta\rho_n$ coincides with the SR characteristics, simply exchanging noise for chaotic fluctuation. Actually, we can say that the weak modulation signal make the system yield SR-like phenomena, exploiting the deterministic fluctuation as noise. Therefore, we call this DSR.

B. Signal to noise ratio (SNR)

Another piece of evidence confirming the SR-like behavior in a deterministic system is given by the SNR as a function of the internal fluctuation. Here, we obtain the SNR from time series data where pulses are placed at the time when phase slips occurred. Figure 7(a) shows the power spectrum of the pulse-train data for $\nu=1.0038$. We can see a high and sharp peak at the external force frequency. This means that the system behaves periodically with fluctuation, in other words, the system synchronizes with the external force statistically. We can also see the higher harmonics of the enhanced signal in the figure at the integer multiples of the modulation signal.

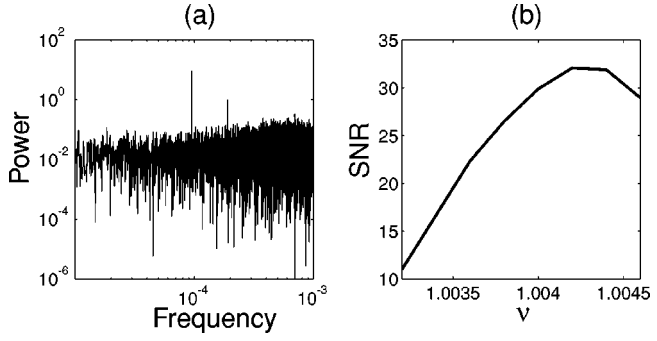

FIG. 7. (a) Power spectrum of pulse-train data for $\nu=1.0038$. A sharp peak is seen at $f\simeq 9.55\times 10^{-5}$, which is the frequency of the external signal. (b) The SNR has a unimodal shape as a function of ν and it is also confirmed that the Rössler system exhibits SR-like behavior in terms of SNR.

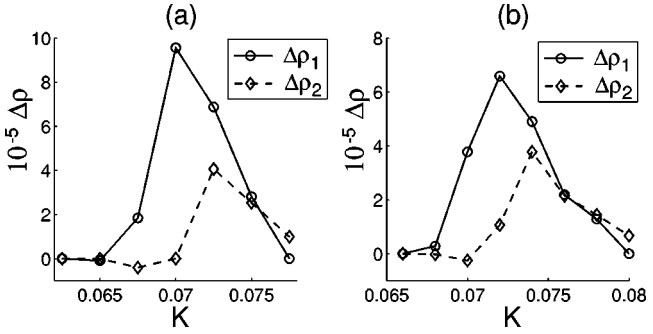

FIG. 8. The peak-height difference with and without a modulation signal for the first peaks $\Delta\rho_1$ and the second peaks $\Delta\rho_2$. (a) The peak-height differences are plotted vs K when ν is modulated and K is used as a controlling parameter. (b) The peak-height differences are plotted vs K when K is modulated as well as used as a controlling parameter. Both curves show the DSR characteristics. This shows that DSR can be observed no matter which bifurcation parameters are employed as modulated and controlling parameters.

The SNR is the power ratio of the signal to the background noise. The power of the enhanced signal is the height of the δ-function-like spike at the external force frequency and the power of the background noise is calculated as the mean power around the δ spike except for its immediate neighborhood. Figure 7(b) shows the SNR as a function of parameter ν. We can see that the SNR increases as ν increases, reaches a maximum value at $\nu=1.0042$, and then decreases in other words, the system exhibits optimal resonance for an appropriate chaotic fluctuation. This coincides with the SR behavior; the existence of DSR is confirmed again in terms of SNR. It should be noted that the optimum resonance is realized for a larger value of ν than that obtained from the peak height differences of the ISID.

C. Controlling and modulated parameters

Thus far, we have chosen ν as a parameter for controlling the internal fluctuation and K as a parameter modulated by the external signal. It is natural to ask which parameters in the systems can be used as controlling and modulated parameters to yield DSR. As described in detail in Sec. IV, ν and K are bifurcation parameters for an unstable-unstable pair bifurcation, which relates to phase slips, and they are equivalent in terms of bifurcation. Here, we demonstrate DSR, using the bifurcation parameters in different role combinations.

First, we exchange the roles of parameters ν and K: ν is modulated by a signal and K becomes the control parameter of the chaotic fluctuation. Figure 8(a) shows the height difference at the first and second peaks in the ISID as a function of K. The DSR in the system is confirmed by the bell-shaped dependence of the height difference on K. DSR can be observed as we expected, even if the roles of the parameters are exchanged. We also examine another choice of parameter roles: K is used as a controlling parameter as well as a modulated parameter. Figure 8(b) plots the peak differences versus K and it can be seen that the system synchronizes best with the external signal for an appropriate K value. We can see DSR even when just one parameter plays both roles. It is

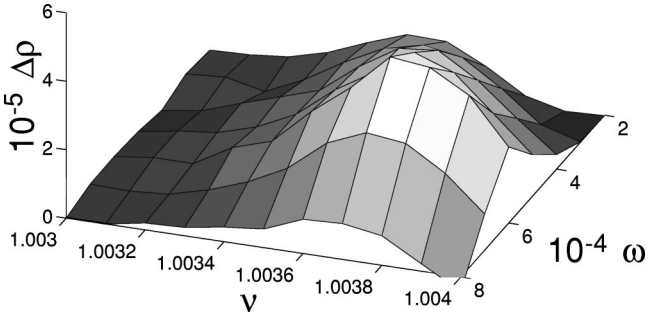

FIG. 9. The peak-height difference with and without a modulation signal as a function of the control parameter ν and the signal frequency ω. The system resonates most with a signal whose frequency is 6.0×10^{-4}.

revealed that DSR can be observed in a system where some bifurcation parameters are modulated and the same or different bifurcation parameters are used to control internal fluctuation.

D. Frequency dependence

We investigated the frequency dependence of DSR. Figure 9 shows the peak-height difference as a function of the controlling parameter ν and the frequency ω of the modulation signal. For each signal frequency, the peak-height difference has a bell-shaped maximum, that is to say, the system exhibits DSR. In addition, the optimum ν value increases slightly as the frequency increases. We can see that the system has the optimum signal frequency for detection. When the modulation signal period is so small, the system hardly resonates with the signal due to the refractory time and, thus, it is thought that the peak heights become low. When the period is too long, the interslip intervals are distributed widely and peaks are thought to be gently sloping.

IV. ANALYSIS OF DETERMINISTIC STOCHASTIC RESONANCE

A. Boundary crisis and unstable-unstable pair bifurcation

In this section, we describe the phase slip in terms of a dynamical system. When the phase of a Rössler oscillator is locked to an external force, trajectories are confined within chaotic attractors in the $(\Delta\theta,r,z)$ space. In this space, there are an infinite array of chaotic attractors, which are arranged in the $\Delta\theta$ direction spaced by 2π because of the invariance of the system (5) to the transformation $\theta\mapsto\theta\pm2\pi$. This means that the phase difference $\Delta\theta$ fluctuates only within a certain range whose width is less than 2π.

A stroboscopic map is useful for visualizing the dynamical processes in a Rössler system. The stroboscopic map **M** is defined by sampling the flow of system (5) at every period of the external force, i.e., $\Delta\theta_i=\Delta\theta(t=2\pi i/\Omega)$, $r_i=r(t=2\pi i/\Omega)$, and $z_i=z(t=2\pi i/\Omega)$, where i is an integer:

$$\mathbf{M}:\mathbf{R}^3\rightarrow\mathbf{R}^3,(\Delta\theta_i,r_i,z_i)\mapsto(\Delta\theta_{i+1},r_{i+1},z_{i+1}). \quad (7)$$

It is shown in Ref. [31] that attractors lie on a near two-dimensional manifold in the $(\Delta\theta,r,z)$ space in the phase

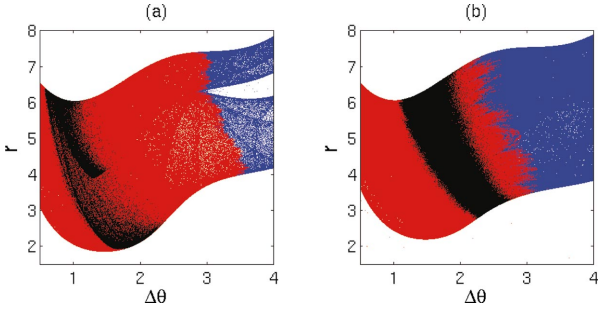

FIG. 10. (Color) (a) Attractor and basins projected on the $(\Delta\theta, r)$ plane when $K=0.15$. The black points represent an attractor and the red points indicate its basin. The blue points show the basin of the next attractor. (b) Attractor remnant and basins where $K=0.085$. The blue points, namely, the basin of the next attractor, touch the black points. In other words, channels connecting the attractor remnants are formed. Trajectories in the black area can escape to next attractor remnant via the channel.

synchronization state. Therefore, in Fig. 10(a) we can clearly see an attractor and basins projected onto the $(\Delta\theta,r)$ plane. Orbits initially distributed in an appropriate region in a $(\Delta\theta,r,z)$ space with the three-dimensional volume approach the two-dimensional manifold within a few cycles [31]. Then, in Fig. 10, we plotted the resulting orbits with the exception of the first few cycles as attractors or as basins. In Fig. 10(a), the black and red points indicate an attractor and its basin, respectively. The blue points show the basin of the next attractor on the right: the blue points on the manifold will move towards the right attractor displaced from the presented one by 2π. There is no path that connects different attractors. In the stroboscopic map, the phase difference $\Delta\theta_i$ is confined within one of these chaotic attractors when the phase is locked to the external force.

When the system is in the desynchronization state, the regions that were previously occupied by isolated attractors,

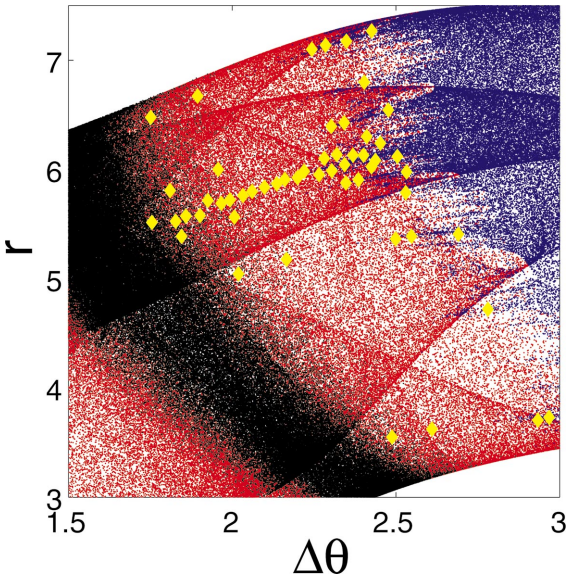

FIG. 11. (Color) The trajectory passing through the channel to the next attractor remnant is plotted with the yellow diamonds ◇. This is an example of phase slip trajectories.

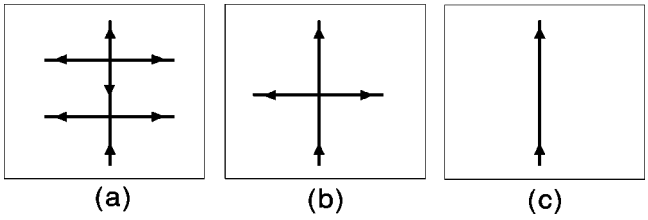

FIG. 12. Process of unstable-unstable pair bifurcation. There are two unstable fixed points (a) and they approach each other. The fixed points coalesce (b). The points have disappeared (c).

which are called the attractor remnants, are connected by certain trajectories. However, when the system is near the bifurcation point, the attractor remnants have shapes that are similar to those of the original attractors and still lies on a near two-dimensional manifold. Near the transition point, we observe the chaotic transient, that is, trajectories stay in an attractor remnants for a long time and then intermittently move to the next attractor remnant via a created path. In Fig. 10(b), we can actually see that the blue region, which was the basin of the next attractor, touches the black region, i.e., the attractor remnant. In other words, paths are created by a boundary crisis: the collision of an attractor with a periodic orbit at its basin boundary [41–43]. Trajectories that experienced the chaotic transient can accidentally land on the blue region and move to the next attractor remnant. This is the phase slips process.

In Fig. 11, the yellow diamonds $\diamondsuit$ moving from left to right represent the trajectory of a phase slip. The trajectory passes through a narrow channel and the channel appears to be the only dominant channel in the parameter range used. The motion of the trajectory indicates that the transition between the phase synchronization state and the phase slip state is caused by an unstable-unstable pair bifurcation [29,31,42]. This bifurcation process is illustrated in Fig. 12. Suppose that there are a saddle and a repeller and the stable manifold of the saddle is identified with the unstable manifold of the repeller, as shown in Fig. 12(a). As the parameter approaches a bifurcation value, these fixed points approach each other. When the parameter coincides with the bifurcation value, the fixed points coalesce, as seen in Fig. 12(b), and then, if the parameter increases through the critical value, the fixed points disappear and a trajectory can move through a channel from right to left, as seen in Fig. 12(c).

In order to reveal the process of an unstable-unstable pair bifurcation in the Rössler oscillator, we used the displacement d_{min} of map $\mathbf{M}$ as a function of $\Delta\theta$:

$$d_{min}(\Delta\theta) = \min_{r,z} \| \mathbf{M}(\Delta\theta, r, z) - (\Delta\theta, r, z) \|, \tag{8}$$

where $\mathbf{M}(\Delta\theta, r, z)$ stands for the image of a point $(\Delta\theta, r, z)$ given by the stroboscopic map $\mathbf{M}$. The behavior of fixed points can be observed via this map since the definition states that d_{min} is zero at a fixed point. Figure 13 shows d_{min} plotted as a function of $\Delta\theta$ for $\nu = 1.0038$ and some Ks. In Fig. 13, there are sharp decreases in d_{min} at two points for a large K, which correspond to fixed points. As K increases, these two fixed points approach each other. The coalescence

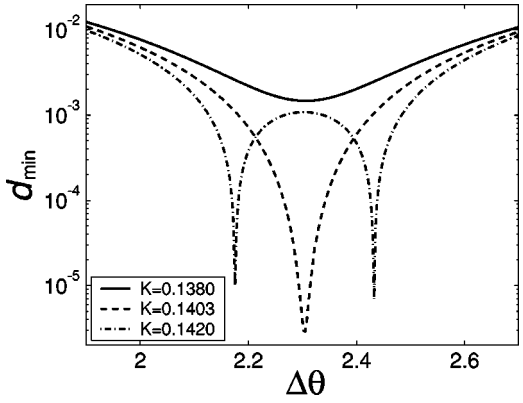

FIG. 13. Displacement map $d_{min} = \min \| \mathbf{M}(\Delta\theta, r, z) - (\Delta\theta, r, z) \|$ is plotted for several K values. The sharp decreases indicate fixed points. There are two fixed points ($K = 0.1420$). The two fixed points coalesce ($K = 0.1403$) and disappear ($K = 0.1380$). This supports the fact that an unstable-unstable pair bifurcation has occurred.

of the two fixed points is observed at $K = 0.1403$, which corresponds to the bifurcation point. With a smaller K, we cannot see any sharp decrease in d_{min}, which means the fixed points have disappeared. This behavior coincides with the unstable-unstable pair bifurcation process and confirms that such bifurcation takes place in the crisis. In addition, we can determine the bifurcation value as $K = 0.1403$ since the displacement map has one sharp decrease at the bifurcation point.

B. Super persistent chaotic transient

Phase slips can occur after the crisis. However, when a system is near a bifurcation point, trajectories experience long term chaotic transients and, therefore, we seldom observe phase slips. Thus, in practice we employ parameter values that are considerably smaller or larger than a critical value to allow us to observe a sufficient number of phase slips in numerical simulations. The long term chaotic transient is called the super persistent chaotic transient and we show why the chaotic transients are so long by deriving the phase slip rate f as a function of bifurcation parameters.

As mentioned above, the crisis is caused by the unstable-unstable pair bifurcation. After the bifurcation, unstable fixed points disappear and channels for the phase slips are developed. However, there are multiplicators near the channels. One multiplicator (approximately in the $\Delta\theta$ direction, which we call the weakly unstable direction) has a value close to one and another (approximately in the r direction, which we call the strongly unstable direction) has an absolute value larger than one, which we denote by μ. The other multiplicator is disregarded since the motion is restricted to the two-dimensional manifold. The dynamics in the weakly unstable direction is the same as that for a usual saddle-node bifurcation. Therefore, for any K, a time t_{sl} needed for a trajectory to pass through the channel in the weakly unstable direction, the so-called laminar length, can be scaled by [43]

$$t_{sl} \sim [K_c(\nu) - K]^{-1/2}. \tag{9}$$

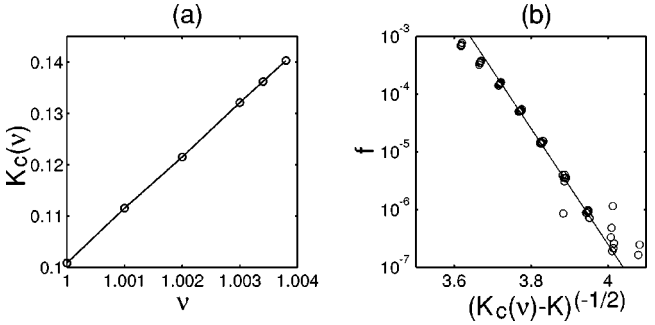

FIG. 14. (a) Plot of the K_c dependence on ν. The dots lie almost all on a straight line. (b) The slip rate against the distance from the bifurcation point is plotted. The dots are almost on the line and this confirms Eq. (13).

It should be noted that the notation $K_c(\nu)$ represents the dependence of K_c on the ν value. When we expand K_c with respect to $\nu-\nu_0$, we have the first-order approximation

$$t_{sl}\sim\left[K_c(\nu_0)+\left.\frac{\partial K_c}{\partial\nu}\right|_{\nu=\nu_0}(\nu-\nu_0)-K\right]^{-1/2}. \tag{10}$$

This expresses the dependence of the laminar length on the bifurcation parameters K and ν. The first-order expansion is indeed a good approximation since K_c relates ν with an almost first-order relationship, as shown in Fig. 14(a).

A phase slip can occur if a trajectory is rather close to the center of a channel. The trajectory is rapidly repelled in the strongly unstable direction while it passes through the channel in the weakly unstable direction. Thus, if the trajectory is so close to the center of the channel that it remains in the channel after t_{sl}, then the phase slip occurs successfully. The distance $\Delta(t)$ of the trajectory from the channel center in the strongly unstable direction grows exponentially with time

$$\Delta(t)\simeq\Delta(0)|\mu|^t. \tag{11}$$

Since the phase slip can occur if $\Delta(t_{sl})$ is smaller than the half-width C_1' of the channel, we have the condition for a phase slip

$$\Delta(0)<C_1'|\mu|^{-t_{sl}}. \tag{12}$$

The trajectory initially has to visit a very small region that satisfies Eq. (12) to pass through the channel. If we assume a uniform invariant probability density in the neighborhood of the channel in the attractor remnant, the probability of the trajectory visiting the above small region during a unit time is also proportional to $C_1'|\mu|^{-t_{sl}}$. This probability gives us the slip rate f. Therefore, using the scaling law Eq. (10) for t_{sl}, we arrive at

$$f(K,\nu)\simeq C_1\exp\left[-C_2\left\{K_c+\frac{\partial K_c}{\partial\nu}(\nu-\nu_0)-K\right\}^{-1/2}\right]. \tag{13}$$

In Fig. 14(b), we plot numerical results for $f(K,\nu)$ determined by the index of the exponential ISID against $[K_c(\nu)-K]^{-1/2}$ for several values of ν. The theoretical result, Eq. (13), is also shown by a solid line. Here, we determine that $\nu_0=1.0034$, $K_c(\nu_0)=0.1362$, and $\partial K_c/\partial\nu=10.25$ from the d_{min} calculations and that $C_1=3.37\times10^{33}$ and $C_2=23.1$ by applying a curve-fitting method to the numerical results of f. The results are in good agreement. This means that the probability of the phase slip decreases exponentially as the parameters approach a bifurcation point. This causes a super persistent chaotic transient.

C. Poisson process with periodic rate

In the previous section, we described the phase slip rate as a function of two bifurcation parameters. Based on this rate, we clarify the DSR mechanism: we derive the behavior of the peak-height difference, which has a bell-shaped maximum as a function of the bifurcation parameters, based on the approximation theory of the time-dependent Poisson process [11,38].

From the numerical simulation, the distribution $\rho(\tau)$ for $\epsilon=0$ can be well fitted to an exponential distribution except when τ is small, i.e., $\rho(\tau)\simeq\lambda_0\exp(-\lambda_0\tau)$ [see Fig. 5(a)]. The exponential form of $\rho(\tau)$ implies that phase slips occur as a Poisson process.

With $\epsilon\neq0$, $\rho(\tau)$ has multipeaks as stated above. We discuss only the case of a slowly varying periodic signal, i.e., $\omega\ll1$. This condition allows us to use an adiabatic approximation: only the rate λ is modulated by the periodic signal. It follows that the occurrence of phase slips obeys a Poisson process with the *time-dependent* rate $\lambda(t)$, which has a period $T=2\pi/\omega$. For the sake of simplifying the notations, we define the following symbols:

$$\int_0^t\lambda(\tau)d\tau=\Lambda(t),\quad\int_0^T\lambda(t)dt=\Lambda(T)=\Lambda,$$

$$\int_0^T\lambda^2(t)dt=\Lambda_2. \tag{14}$$

Suppose that a phase slip occurs at $t=t_0$ and without loss of generality we can take $t_0\in[0,T)$ by shifting the time origin. We introduce the new time variable as $\tau=t-t_0$ and the time-dependent rate is given as a function of τ and t_0, i.e., $\lambda(\tau+t_0)$. The probability distribution that the next phase slip occurs at time τ can be given by

$$P(\tau|t_0)=\lambda(\tau+t_0)\exp\left[-\int_{t_0}^{\tau+t_0}\lambda(t)dt\right]$$

$$=\lambda(\tau+t_0)\exp[-\{\Lambda(\tau+t_0)-\Lambda(t_0)\}]. \tag{15}$$

Suppose that t_1 is in $[0,T)$ and that the time t_1 relates to τ as $\tau+t_0=t_1+mT$, where $m=1,2,\ldots,$ if $t_1<t_0$ and $m=0,1,\ldots,$ if $t_1\geqslant t_0$. If we change the variable τ to t_1 in Eq. (15), we can obtain the probability distribution $P_m(t_1|t_0)$ that the next phase slip occurs at $t_1=\tau+t_0-mT$:

$$P(\tau|t_0)=\lambda(t_1)\exp[-\Lambda(t_1)+\Lambda(t_0)-m\Lambda]\equiv P_m(t_1|t_0). \tag{16}$$

The probability distribution $P(t_1|t_0)$ that a phase slip occurs at t_1 if the previous phase slip occurred at t_0 is given by

$$P(t_1|t_0)=\sum_{m=m_0}^{\infty} P_m(t_1|t_0)=\begin{cases}\lambda(t_1)\exp[-\Lambda(t_1)+\Lambda(t_0)](1-e^{-\Lambda})^{-1}, & t_1\geqslant t_0\\ \lambda(t_1)\exp[-\Lambda(t_1)+\Lambda(t_0)]e^{-\Lambda}(1-e^{-\Lambda})^{-1}, & t_1<t_0,\end{cases} \tag{17}$$

where $m_0=1$ if $t_0>t_1$ and $m_0=0$ if $t_0\leqslant t_1$.

Let $W(t_0)$ be the probability distribution of phase slips for the time t_0+mT, where $t_0\in[0,T)$. In the equilibrium state, $W(t_0)$ has to satisfy the integral equation

$$\begin{aligned}W(t_1)&=\int_0^T P(t_1|t_0)W(t_0)dt_0\\&=(1-e^{-\Lambda})^{-1}\lambda(t_1)e^{-\Lambda(t_1)}\left\{\int_0^{t_1} e^{\Lambda(t_0)}W(t_0)dt_0\right.\\&\left.+e^{-\Lambda}\int_{t_1}^{T} e^{\Lambda(t_0)}W(t_0)dt_0\right\}.\end{aligned} \tag{18}$$

By differentiating both sides, we have

$$\begin{aligned}W'(t_1)&=(1-e^{-\Lambda})^{-1}[\{\lambda'(t_1)-\lambda^2(t_1)\}\\&\times e^{-\Lambda(t_1)}(1-e^{-\Lambda})\lambda^{-1}(t_1)e^{\Lambda(t_1)}W(t_1)\\&=\lambda'(t_1)\lambda^{-1}(t_1)W(t_1).\end{aligned} \tag{19}$$

Finally, with the normalization condition, this can be solved as

$$W(t)=\frac{1}{\Lambda}\lambda(t). \tag{20}$$

Figure 15(a) shows the probability distribution $W(t)$ obtained from the numerical simulations and by Eqs. (20) and (24). The two curves are coincident.

The probability distribution of the interslip interval can be found by averaging the conditional probability distribution $P(\tau|t_0)$ over a period T:

$$\rho(\tau)=\int_0^T P(\tau|t_0)\frac{1}{\Lambda}\lambda(t_0)dt_0. \tag{21}$$

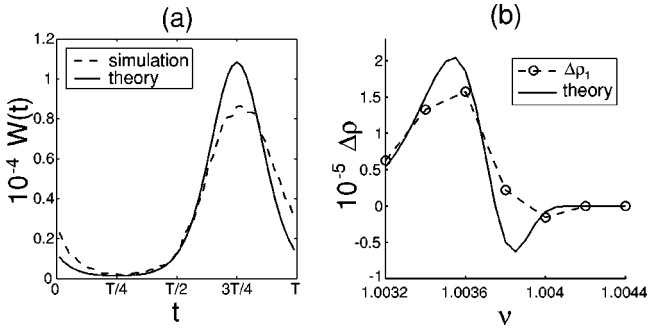

FIG. 15. (a) Plot of the probability distribution $W(t)$ against $t\in[0,T)$ with $\omega=2.0\times10^{-4}$ and $\epsilon=0.05$. (b) Theoretical curve of first peak of ISID obtained by Eqs. (13) and (26) is plotted along with results obtained by the simulation. The good agreement between the two curves confirms the DSR analysis.

Since the nth peak of $\rho(\tau)$ is located at $\tau_n=nT$, we can calculate the nth peak height as

$$\begin{aligned}\rho(\tau_n)&=\frac{1}{\Lambda}\int_0^T\lambda(t_0)\lambda(nT+t_0)\\&\times\exp[-\{\Lambda(nT+t_0)-\Lambda(t_0)\}]dt_0\end{aligned} \tag{22}$$

$$=\frac{1}{\Lambda}\int_0^T\lambda^2(t_0)\exp(-n\Lambda)dt_0=\frac{\Lambda_2}{\Lambda}e^{-n\Lambda}. \tag{23}$$

We consider the system Eq. (6). When the modulation signal is imposed, the time dependence of $\lambda(t)$ arises from the modulation of variable K in $f(K,\nu)$. If we substitute $K[1+\epsilon\sin(\omega\tau+\phi_0)]$, we have

$$\begin{aligned}\lambda(t)&=f(K[1+\epsilon\sin(\omega t)],\nu)\\&=C_1\exp\left\{\frac{-A}{\sqrt{1-\mu\sin(\omega t)}}\right\}\\&\sim C_1\exp\left\{-A\left(1+\frac{\mu}{2}\sin\omega t\right)\right\},\end{aligned} \tag{24}$$

where

$$A=\frac{C_2}{\sqrt{K_c+\dfrac{\partial K_c}{\partial\nu}(\nu-\nu_0)-K}},$$

$$\mu=\frac{\epsilon K}{K_c+\dfrac{\partial K_c}{\partial\nu}(\nu-\nu_0)-K}.$$

We can obtain the ISID $\rho(nT)$ by substituting Eq. (24) into Eq. (23)

$$\rho(\tau_n)=\lambda_0\frac{I_0(A\mu)}{I_0\left(\dfrac{A\mu}{2}\right)}e^{-nT\lambda_0 I_0(A\mu/2)}, \tag{25}$$

where I_0 indicates a modified Bessel function. Without a modulation signal, λ_0 is identified as the phase slip probability distribution $f(K,\nu)$, i.e., $\lambda_0=C_1e^{-A}$. It should be noted that, for $\epsilon=0$, the distribution $\rho(nT;\epsilon=0)=\lambda_0\exp(-nT\lambda_0)$ coincides with $\rho(\tau_n)$ with $\mu=0$ in Eq. (25). If we subtract $\rho(\tau_n;\epsilon=0)$ from $\rho(\tau_n;\epsilon\neq0)$, we obtain the difference $\Delta\rho_n$ in the nth peak height between $\epsilon=0$ and $\epsilon\neq0$ as follows:

$$\Delta\rho_n(\nu) = \lambda_0 \frac{I_0(A\mu)}{I_0\left(\frac{A\mu}{2}\right)} e^{-nT\lambda_0 I_0(A\mu/2)} - \lambda_0 \exp(-nT\lambda_0) \tag{26}$$

$$\sim \frac{3-nT\lambda_0}{16} A^2\mu^2\lambda_0 e^{-nT\lambda_0}. \tag{27}$$

The difference $\Delta\rho_n$ can be regarded as a function of ν. Figure 15(b) shows the theoretical curve of $\Delta\rho_1$ obtained from Eqs. (26) and (13), along with the simulation curve of the first peak difference. Both curves actually show the DSR behavior and there is good agreement between them.

In Eq. (26), the slip rate λ_0 and $A\mu$ are quantities that can be determined in a signal free case ($\epsilon=0$). This indicates that whether or not $\Delta\rho_n$ exhibits DSR behavior depends on the signal free properties of the system. Thus, we can say that if a system yields intermittent events, caused by an unstable-unstable pair crisis, we can observe DSR by choosing appropriate bifurcation parameters for modulations and controls.

V. NOISY DETERMINISTIC STOCHASTIC RESONANCE

In a noisy environment, it is natural that a signal mixed with noise is fed into a system that has the potential to yield DSR effect. Thus, here, let us assume that the system is driven by a periodic force modulated by both a signal and noise, as described by the following equations:

$$\dot{x} = s(y-z),$$

$$\dot{y} = s(x+ay) + K[1+\epsilon\sin(\omega t)+\xi(t)]\sin(\Omega t), \tag{28}$$

$$\dot{z} = s[b+z(x-c)],$$

where ξ is white Gaussian noise: $\langle\xi(t)\xi(t+\tau)\rangle = 2D\delta(\tau)$.

In order to simulate Eq. (28), we can use several well-known methods for solving stochastic differential equations [44,45]. However, higher order methods become complicated, compared with the typical methods used for ordinary differential equations such as the Runge-Kutta method [46]. Moreover, in the noiseless limit, a simulated trajectory has to coincide with a trajectory obtained for ordinary differential equations. Thus, we modify the Runge-Kutta method by introducing a noise term multiplied by the square root of the time step.

Figure 16 shows curves of the first peak differences $\Delta\rho_1$ versus ν for several noise intensities D. Each curve obtained numerically has a bell-shaped maximum. In other words, for a given external noise intensity, the system can effectively detect a weak signal using an appropriate ν value. This means that optimum resonance can be realized by adjusting a parameter even if the system receives a signal with noise of an unknown level. This reveals that even a stochastic system such as Eq. (28) can exhibit DSR-like behavior. Although it is no longer a deterministic system, we regard such a phenomenon as a kind of DSR since we consider that noise happens to be inputed into the system that can yield DSR without noise and call it noisy DSR.

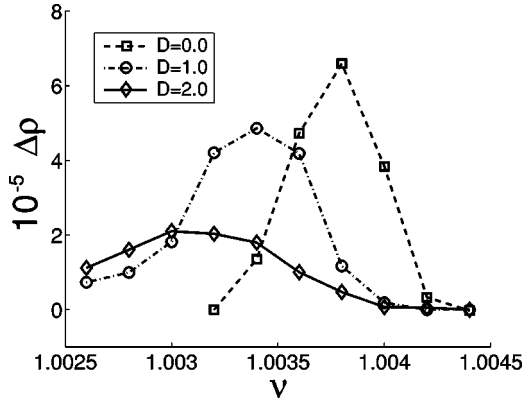

FIG. 16. The first peak difference is plotted vs ν for $D=0.0$, 1.0, and 2.0. For each noise intensity, the difference has a unimodal shape. DSR-like phenomena are observed even if a signal is mixed with noise.

We also observed that if the noise intensity D increases, the maximum points of $\Delta\rho_1$ are shifted to the left, namely, as the noise increases, the optimum ν becomes smaller, i.e., closer to a bifurcation point, and the chaotic fluctuation is suppressed even further. In other words, the most coherent behavior can be achieved by cooperation between the internal fluctuations and the external noise.

VI. CONCLUSION

In a certain parameter region, a Rössler oscillator is phase locked to an external force. If the system deviates from a synchronization regime, phase slips, namely, intermittent increases in the phase difference, are observed. Numerical experiments show that ISID decays exponentially and indicate that phase slips are well-approximated by a Poisson process. Since the phase slip rate is a monotonical function of the parameter values, the parameters are considered to be able to control the chaotic fluctuation. If the amplitude of the driving force is weakly modulated by a periodic signal, the ISID develops multipeaks centered at an integer multiple of the modulation frequency. This means that phase slips statistically synchronize with the modulation signal and we can say that the peak heights represent the degree of synchronization. In addition, the peak-height difference versus the parameter value, which controls the fluctuation intensity, has a bell-shaped maximum. This dependence coincides with the SR characteristics and we can say that our systems exhibit DSR. In addition, the system is shown to exhibit SR characteristics in terms of SNR. We can say that DSR utilizes the instability of a chaotic system to detect a weak signal, instead of noise. We then considered the roles of the parameters in modulation and control, and the frequency dependence of the external signal.

Next, we explained the bell-shaped dependence of the peak height versus the bifurcation parameter values in terms of a boundary crisis and a time dependent Poisson process. The phase synchronization was shown to be broken by a boundary crisis induced by an unstable-unstable pair bifur-

cation. Based on this fact, we derived the slip rate as a function of the bifurcation parameters. With a modulation signal, the multipeaks in ISID can be explained by the approximation of the phase slips as a Poisson process with a periodic rate. In addition, we showed that the analytically derived peak-height difference agrees well with that obtained by numerical simulations. We believe that the deviations between the theoretical and experimental curves in Fig. 15 were caused by some of the approximations and the precision of the numerical simulations. One piece of evidence supporting our hypothesis is the tendency for slower and smaller modulation signals to form the curves closer to each other. These analytical results show that DSR can be yielded by the system after a boundary crisis if bifurcation parameters are periodically modulated and the same or different bifurcation parameters are employed to control the chaotic fluctuation. Furthermore, since some scaling laws for intermittent event rates versus the bifurcation parameters are known depending on the type of crisis, we can predict the DSR behavior of such kinds of systems by employing the same approaches.

We also demonstrated DSR in a noisy environment since it is important to consider real-world situations. In this case, a signal becomes mixed with noise as it passes through a noisy environment, in other words, the parameter of a system is modulated by noise as well as the signal. Numerical simulation shows that the ISID also has multipeaks in the same way as noiseless systems. In addition, for given noise intensities, the peak-height difference exhibits a unimodal dependence as a function of the controlling parameter. This shows that our systems exhibit DSR-like behavior in a noisy environment, namely, noisy DSR. Even if the external noise level is unknown, we can achieve the maximum enhancement of a signal buried in noise by adjusting the parameters. We can say that the collaboration between instability and noise allows us to detect weak signals.

[1] R. Benzi, A. Sutera, and A. Vulpiani, J. Phys. A **14**, L453 (1981).

[2] R. Benzi, G. Parisi, A. Sutera, and A. Vulpiani, Tellus **34**, 10 (1982).

[3] R. Benzi, A. Sutera, G. Parisi, and A. Vulpiani, SIAM (Soc. Ind. Appl. Math.) J. Appl. Math. **43**, 565 (1983).

[4] L. Gammaitoni, P. Hänggi, P. Jung, and F. Marchesoni, Rev. Mod. Phys. **70**, 223 (1998).

[5] F. Moss, D. Pierson, and D. O'Gorman, Int. J. Bifurcation Chaos Appl. Sci. Eng. **4**, 6 (1994).

[6] K. Wiesenfeld and F. Jaramillo, Chaos **8**, 539 (1998).

[7] A.R. Bulsara and L. Gammaitoni, Phys. Today **49**(3), 39 (1996).

[8] J.K. Douglass, E.P.L. Wilkens, and F. Moss, Nature (London) **365**, 337 (1993).

[9] R. Fitzhugh, Biophys. J. **1**, 445 (1961).

[10] J. Nagumo, S. Arimoto, and S. Yoshizawa, Proc. IRE **50**, 206 (1962).

[11] K. Wiesenfeld, D. Pierson, E. Pantazelou, C. Dames, and F. Moss, Phys. Rev. Lett. **72**, 2125 (1994).

[12] A. Longtin and D.R. Chialvo, Phys. Rev. Lett. **81**, 4012 (1998).

[13] E. Ippen, J. Lindner, and W.L. Ditto, J. Stat. Phys. **70**, 437 (1993).

[14] G. Nicolis, C. Nicolis, and D. McKernan, J. Stat. Phys. **70**, 125 (1993).

[15] T.L. Carroll and L.M. Pecora, Phys. Rev. Lett. **70**, 576 (1993).

[16] T.L. Carroll and L.M. Pecora, Phys. Rev. E **47**, 3941 (1993).

[17] V.S. Anishchenko and M.A. Safanova, Int. J. Bifurcation Chaos Appl. Sci. Eng. **2**, 397 (1992).

[18] V.S. Anishchenko, M.A. Safanova, and L.O. Chua, Int. J. Bifurcation Chaos Appl. Sci. Eng. **4**, 441 (1994).

[19] V.S. Anishchenko, A.B. Neiman, and M.A. Safanova, J. Stat. Phys. **70**, 183 (1993).

[20] S. Sinha and B.K. Chakrabarti, Phys. Rev. E **58**, 8009 (1998).

[21] M. Franaszek and E. Simiu, Phys. Rev. E **54**, 1298 (1996).

[22] C. Eichwald and J. Walleczek, Phys. Rev. E **55**, R6315 (1997).

[23] E. Reibold, W. Just, J. Becker, and H. Benner, Phys. Rev. Lett. **78**, 3101 (1997).

[24] A.N. Pisarchik and R. Corbalán, Phys. Rev. E **58**, R2697 (1998).

[25] K. Arai, K. Yoshimura, and S. Mizutani, Phys. Rev. E **65**, 015202 (2002).

[26] T. Kapitaniak, Phys. Rev. E **49**, 5855 (1994).

[27] M.G. Rosenblum, A.S. Pikovsky, and J. Kurths, Phys. Rev. Lett. **76**, 1804 (1996).

[28] T. Yalçinkaya and Y.C. Lai, Phys. Rev. Lett. **79**, 3885 (1997).

[29] A. Pikovsky, G. Osipov, M.G. Rosenblum, M. Zak, and J. Kurths, Phys. Rev. Lett. **79**, 47 (1997).

[30] A. Pikovsky, M. Zaks, M.G. Rosenblum, G. Osipov, and J. Kurths, Chaos **7**, 680 (1997).

[31] E. Rosa, Jr., E. Ott, and M.H. Hess, Phys. Rev. Lett. **80**, 1642 (1998).

[32] K.J. Lee, Y. Kwak, and T.K. Lim, Phys. Rev. Lett. **81**, 321 (1998).

[33] L. Gammaitoni, F. Marchesoni, E. Menichella-Saetta, and S. Santucci, Phys. Rev. Lett. **62**, 349 (1989).

[34] T. Zhou and F. Moss, Phys. Rev. A **41**, 4255 (1990).

[35] A. Longtin, A. Bulsara, and F. Moss, Phys. Rev. Lett. **67**, 656 (1991).

[36] T. Zhou, F. Moss, and P. Jung, Phys. Rev. A **42**, 3161 (1990).

[37] L. Gammaitoni, F. Marchesoni, and S. Santucci, Phys. Rev. Lett. **74**, 1052 (1995).

[38] M.H. Choi, R.F. Fox, and P. Jung, Phys. Rev. E **57**, 6335 (1998).

[39] J.J. Collins, C.C. Chow, and T.T. Imhoff, Phys. Rev. E **52**, R3321 (1995).

[40] I. Goychuk, Phys. Rev. E **64**, 021909 (2001).

[41] C. Grebogi, E. Ott, and J.A. Yorke, Phys. Rev. Lett. **48**, 1507 (1982).

[42] C. Grebogi, E. Ott, and J.A. Yorke, Phys. Rev. Lett. **50**, 935 (1983).

[43] E. Ott, *Chaos in Dynamical Systems* (Cambridge University Press, Cambridge, 1993).

[44] P.E. Kloeden and E. Platen, *Numerical Solution of Stochastic Differential Equations* (Springer, New York, 1992).

[45] P.E. Kloeden, E. Platen, and H. Schurz, *Numerical Solution of SDE through Computer Experiments* (Springer, New York, 1994).

[46] W.H. Press, B.P. Flannery, S.A. Teukolsky, and W.T. Vetterling, *Numerical Recipes in C* (Cambridge University Press, Cambridge, 1988).